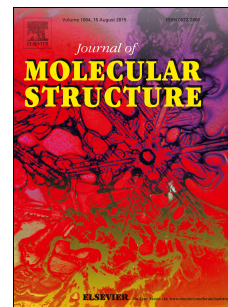


Accepted Manuscript

Synthesis, spectroscopic, computational and drug docking studies of 1-(benzenesulfonyl)-2-methyl-1*H*-indole-3-carbaldehyde

Yagna Narayana Bellomkond, S.P. Vijaya Chamundeeswari



PII: S0022-2860(18)31502-3

DOI: <https://doi.org/10.1016/j.molstruc.2018.12.069>

Reference: MOLSTR 26006

To appear in: *Journal of Molecular Structure*

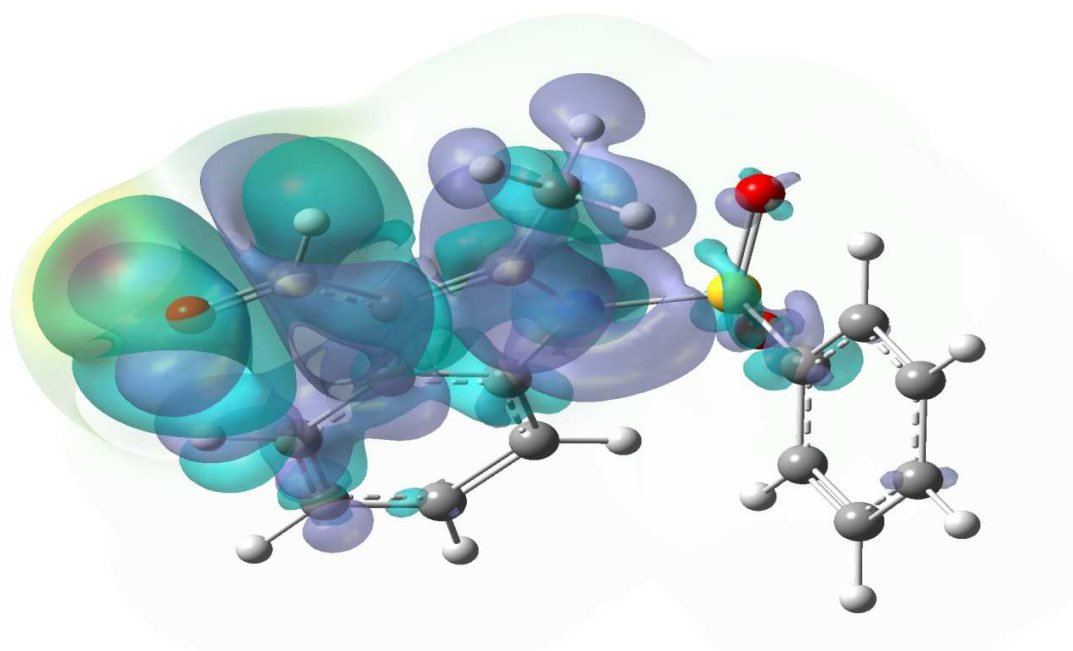
Received Date: 17 July 2018

Revised Date: 14 December 2018

Accepted Date: 17 December 2018

Please cite this article as: Y.N. Bellomkond, S.P. Vijaya Chamundeeswari, Synthesis, spectroscopic, computational and drug docking studies of 1-(benzenesulfonyl)-2-methyl-1*H*-indole-3-carbaldehyde, *Journal of Molecular Structure* (2019), doi: <https://doi.org/10.1016/j.molstruc.2018.12.069>.

This is a PDF file of an unedited manuscript that has been accepted for publication. As a service to our customers we are providing this early version of the manuscript. The manuscript will undergo copyediting, typesetting, and review of the resulting proof before it is published in its final form. Please note that during the production process errors may be discovered which could affect the content, and all legal disclaimers that apply to the journal pertain.

Graphical Abstract**Synthesis, spectroscopic, computational and drug docking studies of
1-(Benzenesulfonyl)-2-Methyl-1H-Indole-3-Carbaldehyde**B.YAGNA NARAYANA*^a and SP.VIJAYA CHAMUNDEESWARI*^a^a *School of Advanced Sciences, Vellore Institute of Technology, Vellore, India.*

Synthesis, spectroscopic, computational and drug docking studies of 1-(Benzenesulfonyl)-2-Methyl-1*H*-Indole-3-Carbaldehyde

Yagna Narayana Bellomkond^a and SP.VijayaChamundeeswari^{b*}

^a School of Advanced Sciences, Vellore Institute of Technology, Vellore, India.

^b Center for crystal Growth, Vellore Institute of Technology, Vellore, India

* E-mail address: vijaya_vit64@yahoo.co.in

Mobile: +91 9003508929

Abstract

An N-Substituted 1*H*-indole derivative having an empirical formula C₁₆H₁₃NO₃S was synthesized by the condensation of 2-Methyl-1*H*-Indole-3-carbaldehyde and benzene sulfonyl chloride in presence of a phase transfer catalyst of type quaternary ammonium salt in basic conditions. Then the compound was characterized by using FT-IR, UV-Visible and NMR spectroscopic methods. Thus the obtained experimental results were effectively compared with DFT studies in arriving the structural characteristics of the title compound. From vibrational analysis, it was observed that carbonyl frequency is somewhat lower than a typical aldehydic stretching frequency and it could be possible only when the formyl group is coplanar with the ring and subsequent resonance conjugation reduces its force constant. Similarly, the optical absorption behavior of a typical indole ring suffered from a bathochromic shift due to the presence of ring substituents. Finally, the molecular drug docking studies of the title compound were performed using AutoDock 4.2 tools to ascertain its binding mode, efficiency and the nature of chemical interactions with the target proteins and it has been predicted theoretically that the binding efficiency of the ligand on the target receptor surface was found to be better in the case of Gram positive bacteria *S.Aureus* than the Gram negative *N.Meningitidis*.

Keywords: 1-Benzenesulfony-1*H*-indole; 3-formyl-1*H*-indole; N-substituted-1*H*-indole; N-substituted sulfonamide; Skatole.

1. Introduction

In the search for safer and more potent therapeutic agents, a popular approach is to synthesize and evaluate biologically active compounds with chemical structures analogous to those having the desired biological activity. The approach of the practice of medicinal field has been developed by synthesizing new compounds based largely on modifications of structures of known activity. Literature survey reveals that majority of the pharmacologically active agents are heterocyclic compounds [1]. Especially, the chemistry of indoles are quite rewarding from synthetic and biological aspects [2-9]. Indole itself is found in coal-tar. Animal body contains indole which is formed along with pus and also in liver, pancreas, the brain and bile. Human and animal faeces are found to contain indole and its methyl homologue i.e. skatole [10].

In view of these general observations, our attention was drawn towards the synthesis and study of biological properties of N-Heterocycles, mainly indole derivatives of biological and pharmacological interest since it has various activities mainly shown to exhibit anti-bacterial properties against Gram positive, Gram negative and fungi [11-12]. Of several natural products containing indole nucleus, mention may be made of the essential amino acid L-tryptophan, the plant growth hormone indole-3-acetic acid, the vasoconstrictor serotonin, a large number of alkaloids like abrine, reserpine, bufotenin, brucine, yohimbine, strychnine etc. Also the medicinally important antibiotics like mitomycin, indolomycin, gliotoxin and aparantoin. As most of the naturally occurring heterocycles possess varieties of pharmacological activities, it is not surprising to expect

that synthetic heterocycles may also exhibit interesting pharmacological properties. For example, the discovery of indomethacin 950, a very important nonsteroidal anti-inflammatory and antipyretic agent gave an impetus to synthesize large number of its structural analogues [13]. Keasling *et al.* have reported that a considerable number of 3-acylindole possessed anticonvulsant action that can be compared to the activity of phenobarbital [14]. Similarly, the various 3-carboxamido-1-phenylindoles also shown to have exhibited analgesic, anti-inflammatory, hypotensive, vaso-dilator, anti-convulsant, sedative, muscle relaxant and para sympatholytic activities. Because of varied biodynamic properties of indole and its derivatives, today the scope of indole research is multifarious extending from rather simple molecules to highly complex molecules. Design and developing a procedure for the transformation of simple molecules into a bioactive molecule with different functionalities is a worthwhile contribution in organic synthesis and thereby we can enhance some important physicochemical properties demanded for a targeted drug delivery. The physicochemical properties of the lead molecule play a critical role in drug formulation. The two most relevant physicochemical properties to drug delivery is solubility and stability. There are several parameters that affect the solubility and chemical stability of a drug in solution. The pH of the solution can dramatically affect both the solubility and chemical stability of the drug. Buffer concentration/composition and ionic strength can also have an effect, especially on chemical stability. The hydrophobic/hydrophilic nature of the drug influences solubility. A typical characterization of a drug will start with a study of the chemical stability of the drug as a function of pH. First, we presented here a report of valid synthetic procedure and the structural analysis drawn out of both experimental and theoretical outcomes. Then, we presented only the theoretical docking results for future considerations regarding biological activity of the title compound.

2. Experimental methods

2.1. Synthesis of 1-(Benzenesulfonyl)-2-Methyl-1*H*-Indole-3-Carbaldehyde

To a solution of 2-Methyl-indole-3-carbaldehyde (**1**) (2.1g, 10.0mmoles) in Benzene (50 mL) containing 50% NaOH solution (25 mL), tetrabutylammonium hydrogensulphate (100 mg) and *P*-Toluenesulfonyl chloride (1.31g, 10.0mmoles) were added. The mixture was stirred well for 4 h. Then it was poured over crushed ice and extracted with ethyl acetate (3x50mL). The organic layer was separated, washed with water (3x25mL) and dried (MgSO₄). Crystallization process by slow solvent evaporation technique using ethyl acetate gave the desired product in 87% yield. The above proposed reaction scheme is presented in **Figure 1**.

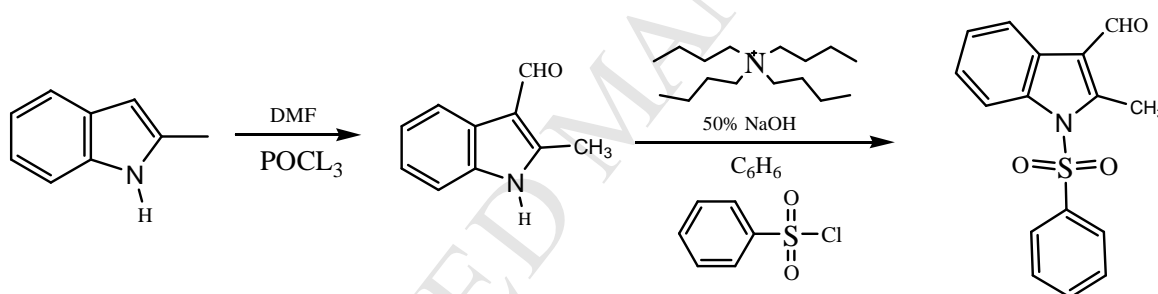


Figure 1. Reaction scheme for the synthesis of 1-(Benzenesulfonyl)-2-Methyl-1-*H*-Indole-3-Carbaldehyde

2.2. FT-IR spectroscopy

The FT-IR spectrum was recorded with Perkin Elmer spectrum One FT-IR spectrometer and the scan range was maintained within the standard limit between the sample and the reference.

2.3. UV-Visible spectroscopy

UV-Visible spectrum of an aqueous solution of the title compound, and deionized water as an internal standard, was recorded over a range of 200–800 nm with a JASCO

V-670 PC spectrophotometer, operated at a resolution of 0.5 nm. The sampling were made in a quartz cuvette having a path length of 1.0 cm.

2.4. ^1H NMR spectroscopy

The ^1H NMR spectrum of the title compound was recorded on Bruker 400 MHz Avance NMR spectrometer using TMS as an internal standard. Sampling of the compound was done by employing polar aprotic solvent, CDCl_3 .

2.5. ^{13}C NMR spectroscopy

The proton decoupled ^{13}C NMR spectrum was recorded on Bruker 400 MHz Avance NMR spectrometer, by using deuterated Chloroform (CDCl_3) as a solvent and TMS was used as an internal standard.

3. Computational methods

3.1. Density Functional Theoretical method

The Density functional theoretical (DFT) calculations were performed using Gaussian-03 quantum-chemical software package [15]. The CAM-B3LYP/B3LYP hybrid density function and triple split valence 6-311++G (d p) basis set has been used [16-18]. It is noteworthy to mention that the original CAMB3LYP functional is defined with a coulomb-attenuating parameter of $\alpha+\beta=0.65$ and, therefore, exhibits a $-0.65/r$ dependence for the exchange potential. As a result, the CAMB3LYP functional becomes different when compared to other LC functionals like LC-BLYP, Wb97xD etc., and it does not incorporate a full 100% HF exchange at large inter-electronic distances [19-20]. The electronic absorption spectrum and the nuclear magnetic shielding tensors were simulated by employing Time-dependent self-consistent field (TD-SCF) and Gauss independent atomic orbital (GIAO) methods [21-22] respectively.

3.2. Molecular drug-docking studies

Docking calculations were carried out using **AutoDock 4.1** tools [23]. Gasteiger partial atomic charges were added to the ligand atoms. Non-polar H-atoms were merged, and rotatable bonds were defined. Docking calculations were carried out on appropriate protein targets. Essential hydrogen atoms, Kollman united atom type charges, and solvation parameter were added with the aid of AutoDock tools. Affinity grid maps of xx Å grid points and 0.375 Å spacing were generated by customizing and running the Autogrid program. AutoDock parameter set- and distance-dependent dielectric functions were used in the calculation of the van der Waals and the electrostatic terms, respectively.

Docking simulations were performed using the Lamarckian genetic algorithm (LGA) and local search method. Initial position, orientation, and torsion of the ligand molecules were set accordingly. All rotatable torsion were released during docking. Each docking experiment was derived from 10 different runs that were set to terminate after a max. of 250000 energy evaluation. The population size was set to 150. During the search, a translational step of 0.2 Å, and quaternion and torsion steps of 5 were applied. Docking results were analyzed and the high-resolution images were generated with the help of CHIMERA molecular visualization program [24].

4. Results and discussion

4.1. Optimized molecular geometry

The geometry minimization, of pre-optimized structure of 1-(Benzenesulfonyl)-2-Methyl-1*H*-Indole-3-Carbaldehyde by semi-empirical method, is carried out using the DFT model CAM-B3LYP/6-311++G (d p) incorporating water as a solvent molecules by utilizing the polar continuum model (PCM) [25-26]. The optimized geometry is shown in the **Figure 2**. Calculated geometrical parameters viz. Bond lengths

and angles are listed in the **Table 1**. The CAM-B3LYP model predicted a ground state energy of about -1295.90 Hartrees in aqueous phase. The gas phase single point energy state of the above mentioned optimized structure of 1-(Benzenesulfonyl)-2-Methyl-1*H*-Indole-3-Carbaldehyde is found to be less stabler than the solvated title compound by means of 100.4 kcal. After 23 states of minimization process in aqueous solution, the stationary point was found and the optimization convergence plot of energy E vs N steps is given in the **Figure 3**. Criteria for convergence to a stationary point is given in the **Table 2**. Similarly, the frequency calculation has no imaginary frequencies which also confirmed that the optimized geometry of the title compound become the stationary point for the molecular system [27].

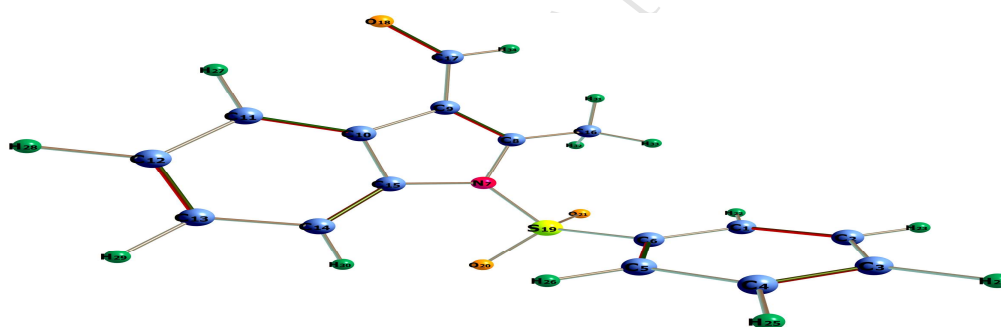


Figure 2. Optimized geometry of 1-(Benzenesulfonyl)-2-Methyl-1*H*-Indole-3-Carbaldehyde showing numbering scheme according to DFT model

The optimized structure shows a co-planar formyl group with an indole ring which could result in an extensive conjugation and it is confirmed from the bond length of 1.45 Å between C₇-C₁₉ atoms. The predicted bond length reveals a partial double bond character between the above mentioned atoms. Furthermore, the C=O bond of formyl group also shows a slight increase in its length, and strongly added support to the bond resonance. Of all C-H bonds, the formyl C-H bond length is found to be higher i.e. proton become deshielded and will expected to have higher chemical shift value compared to other

protons in the title compound. Similarly, an intermediate value of 1.4 Å for C-N bond lengths of indole ring also confirmed the resonance delocalization. The bond lengths of C-S and S=O are found to be 1.8 and 1.4 Å, respectively and showed a good correlation with that of literature value [28] corresponding to σ_{C-S} and $\pi_{S=O}$ bonds. Moreover, both the phenyl and indole ring systems are almost perpendicular to each other, which is evident from the calculate bond angle of about 105° between the C₆-S₁₉-N₇ atoms.

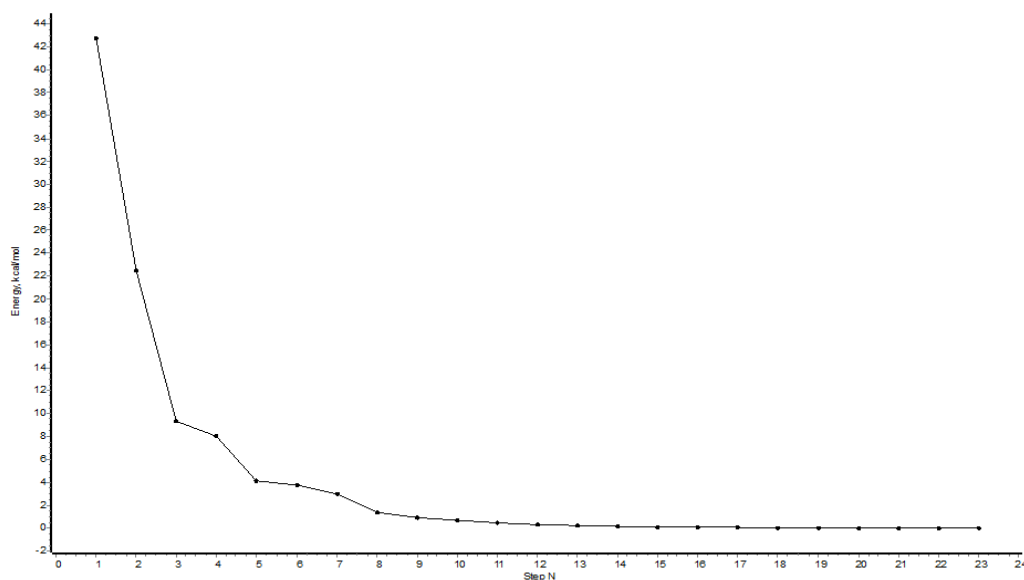
Table 1. Optimized geometrical parameters of 1-(Benzenesulfonyl)-2-Methyl-1*H*-Indole-3-Carbaldehyde by using the CAM-B3LYP/6-311++G (d p) model

Parameters	Obtained values (Å)	Parameters	Obtained values (°)	Parameters	Obtained values (v)
R(1-2)	1.388	R(17-18)	1.219	A(7-19-20)	105.3
R(1-6)	1.388	R(17-34)	1.101	A(7-19-21)	106.8
R(1-22)	1.082	R(19-20)	1.448	A(9-8-16)	128.4
R(2-3)	1.388	R(19-21)	1.447	A(8-9-10)	108.3
R(2-23)	1.082	A(2-1-6)	118.5	A(8-9-17)	125.2
R(3-4)	1.391	A(2-1-22)	121	A(8-16-31)	109.9
R(3-24)	1.083	A(1-2-3)	120.1	A(8-16-32)	111.2
R(4-5)	1.385	A(1-2-23)	119.6	A(8-16-33)	111.4
R(4-25)	1.082	A(6-1-22)	120.4	A(10-9-17)	126.5
R(5-6)	1.39	A(1-6-5)	122.2	A(9-10-11)	132.7
R(5-26)	1.082	A(1-6-19)	118.9	A(9-10-15)	107.3
R(6-19)	1.775	A(3-2-23)	120.3	A(9-17-18)	124.1
R(7-8)	1.396	A(2-3-4)	120.5	A(9-17-34)	116.4
R(7-15)	1.42	A(2-3-24)	119.8	A(11-10-15)	119.9
R(7-19)	1.712	A(4-3-24)	119.7	A(10-11-12)	118.6
R(8-9)	1.373	A(3-4-5)	120.1	A(10-11-27)	119.9
R(8-16)	1.489	A(3-4-25)	120.2	A(10-15-14)	121.8
R(9-10)	1.446	A(5-4-25)	119.6	A(12-11-27)	121.4
R(9-17)	1.447	A(4-5-6)	118.5	A(11-12-13)	120.7
R(10-11)	1.396	A(4-5-26)	120.5	A(11-12-28)	119.8
R(10-15)	1.401	A(6-5-26)	121	A(13-12-28)	119.5
R(11-12)	1.383	A(5-6-19)	118.9	A(12-13-14)	121.6
R(11-27)	1.081	A(6-19-7)	104.7	A(12-13-29)	119.6
R(12-13)	1.398	A(6-19-20)	109.5	A(14-13-29)	118.9
R(12-28)	1.083	A(6-19-21)	109.1	A(13-14-15)	117.4
R(13-14)	1.385	A(8-7-15)	109.2	A(13-14-30)	120.7
R(13-29)	1.083	A(8-7-19)	125.3	A(15-14-30)	121.9
R(14-15)	1.391	A(7-8-9)	108.3	A(31-16-32)	108.9
R(14-30)	1.078	A(7-8-16)	123.4	A(31-16-33)	107.8
R(16-31)	1.086	A(15-7-19)	124.9	A(32-16-33)	107.6
R(16-32)	1.089	A(7-15-10)	106.9	A(18-17-34)	119.5
R(16-33)	1.091	A(7-15-14)	131.3	A(20-19-21)	120.3

R – bond length (Å); A – bond angle (°); W – vibrational frequencies (v).

Table 2. Criteria for the convergence of minimization process

S.No	PARAMETERS	VALUE	THRESHOLD	CONVERGED
1	Max. force	0.000020	0.000450	yes
2	RMS force	0.000004	0.000300	yes
3	Max. displacement	0.001474	0.001800	yes
4	RMS displacement	0.000411	0.001200	yes

**Figure 3.** Optimization convergence plot simulated out of CAM-B3LYP/6-311++G (d,p) model

4.2. Molecular properties

4.2.1 Dipole moment

Dipole moment of 1-(Benzenesulfonyl)-2-Methyl-1*H*-Indole-3-Carbaldehyde is found to be 7.9 D in water, and the respective dipole moment vector components are given in the **Table 3**. In the gas phase, the dipole moment of single point geometry of the title compound is only about 6.0 D which is appreciably lesser than that of the same in aqueous phase and far greater than that of water ($\mu_{\text{total}}=1.85$ D). It seems that the dipole moment of

the title compound could increase with increasing the solvent polarity. Moreover, the overall dipole moment vector is found to be bisecting the XZ-plane from the origin at an approximate angle of 45° and very much perpendicular to Y-axis, is shown in **Figure 4**.

Table 3. Theoretical dipole moment and dipole moment components of 1-(Benzenesulfonyl)-2-Methyl-1*H*-Indole-3-Carbaldehyde

<i>Dipole vector components</i>	Dipole moment, μ (Debye)
μ_x	-6.89
μ_y	0.47
μ_z	-3.82
μ_{total}	7.90

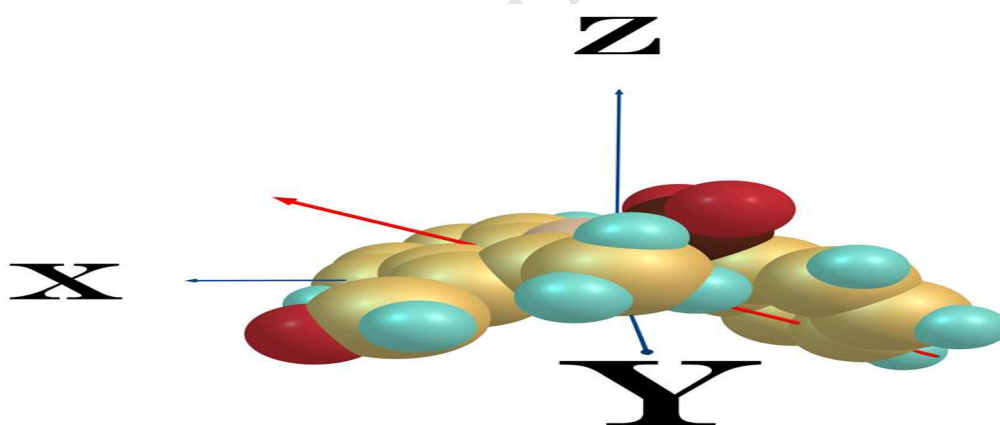


Figure 4. Space-fill geometry of the compound showing the overall dipole moment vector on the Cartesian axes

4.2.2 Molecular electrostatic potential (MEP)

Molecular electrostatic potential map provides versatile information about the molecular reactivities such as nucleophilicity, electrophilicity, protonation/deprotonation, H-bonding's and various other possible molecular interactions [29]. The MEP surfaces of 1-(Benzenesulfonyl)-2-Methyl-1*H*-Indole-3-Carbaldehyde is shown in **Figure 5**. As expected, most electronegative atoms viz. C and N-atoms has a negative potential surface indicated by bright red colored surface. Indole N-atom has comparatively less negative

potential than that of O-atoms, since its lone pair of electrons involved in an aromatic delocalization. Hence, the three O-atoms only expected to be participate in any kind of inter-molecular interactions. The sulfonyl S-atom seems buried inside the highest possible positive potential surface of the title compound.

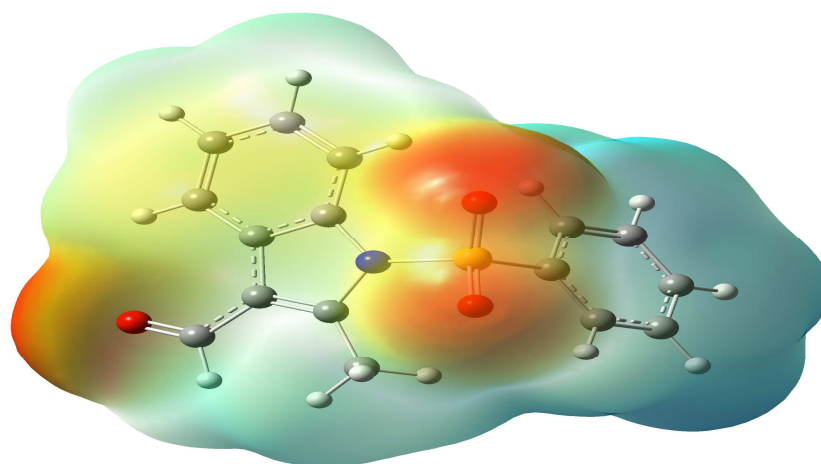


Figure 5. MEP Surface of 1-(Benzenesulfonyl)-2-Methyl-1*H*-Indole-3-Carbaldehyde

4.2.3 FMO Analysis

Frontier molecular orbital analysis of the title compound is carried by using the same DFT model as mentioned earlier for geometry optimization. The molecular system found to have 219 molecular orbitals. Among them only 156 orbitals are comprising of bonding and anti-bonding orbital. Rest of them are Rydberg and Non-bonding lone pair orbitals. Both HOMO and LUMO has anti-symmetric properties with energy of about -7.9 and -0.76 e V, respectively. The calculated energy gap is found to be quiet large, 7.13 e V. **Figure 6a & b**, shows the frontier molecular orbitals of 1-(Benzenesulfonyl)-2-Methyl-1*H*-Indole-3-Carbaldehyde. Evidently, the HOMO is a pi-bonding molecular orbital with occupancy of 1.69 on the C-atoms of the indole ring at position-11 and 12. Whereas LUMO mainly centered on the Rydberg orbitals of the ring carbon atoms with p-

character at position-1 and 2. It seems very hard for an excitation to happen between these two states due to an unfavorable energy criteria under ordinary conditions.

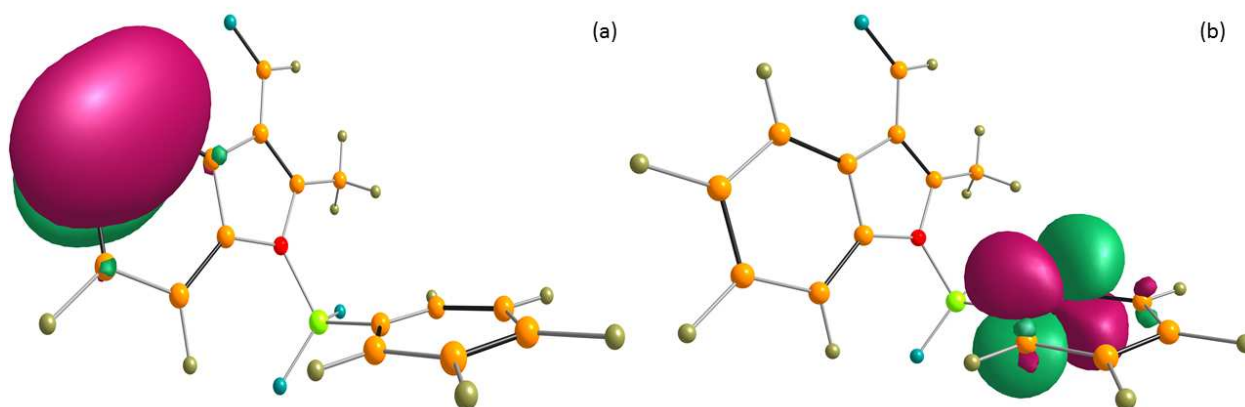


Figure 6a. HOMO and b. LUMO of 1-(Benzenesulfonyl)-2-Methyl-1H-Indole-3-Carbaldehyde

4.3. NPA and NBO Analysis

For NPA and NBO analysis [30], the pre-optimized structure of 1-(Benzenesulfonyl)-2-Methyl-1H-Indole-3-Carbaldehyde obtained from CAM-B3LYP/6-311++G (d p) is utilized. The chosen triple split valence basis model consists of 219 AOs (9 AOs each on C,N and O; 13 on S-atom; 2 on each H-atom) extended by 93 AOs beyond the minimum basis level.

4.3.1 NPA Analysis

From NAO population, it is observed that carbonyl C-atom possesses a minimum valence 2s orbital Lewis pair occupancy of only about 0.9 whereas the valence 2s orbital of O-atom contains a maximum orbital occupancy of about 1.70. Here, the carbonyl C-atom showed a depletion of 6% of its electron density which can make it as a potent nucleophilic center and the carbonyl O-atom gains an extra population of about 7.25% of its own electron density. Also, the formyl H-atom contains a least energetic valence 1s

orbital of maximum occupancy 0.82. Similarly, the N-atom of indole ring has a total occupancy of 7.61 which is slightly greater than its actual occupancy. Here the N-atom could have gained its extra population during aromatic delocalization of pi-electrons. The S-atom of sulfonyl group found to have a total occupancy of only about 13.73 out of 16. Depletion of electron densities could arise due to the presence of two more electronegative O-atoms.

The summary of NPA in terms of atomic charge distribution is shown in **Figure 7**. The sulfonyl S-atom has nuclear charge of about 2.265 which is far greater than the charge on the nucleophilic carbonyl C-atom having the value of 0.36. Higher nuclear charge on the S-atom could arise due to more electronegative O- and N-atom to which the former is attached tetrahedrally. All the ring C-atoms, except those attached directly to the more electronegative N-atom, have negative atomic charges reflecting extra population on their corresponding atomic orbitals. As expected, all electronegative atoms viz. N and O's possess negative atomic charges. Amongst the sulfonyl O-atoms has large negative value. Similarly, the Natural Minimal Basis (NMB) and Natural Rydberg Basis (NRB) populations of 1-(Benzenesulfonyl)-2-Methyl-1*H*-Indole-3-Carbaldehyde are presented in the **Table 4**. It is evident that ninety three Rydberg orbitals of the NRB set contribute only 0.2% of electron density. As expected, NMB account for a maximum of 97.79% of electron densities in the molecule.

Table 4. Summary of the NMB and NRB populations

S.No	TYPE	TOTAL POPULATION
1	Core	99.96% of 50
2	Valence	99.71% of 106
3	Natural Minimal Basis	99.79% of 156
4	Natural Rydberg Basis	0.21% of 156

of N-atom and the anti-bonding orbitals of C₈-C₉ and C₁₀-C₁₅ provides a delocalization energies of about 44.5 and 29.7 kcal, respectively. Similarly, the three lone pair occupancies on each O-atom of sulfonyl bond found to be involved in a transition to an anti-bonding orbitals of N₇-S₁₉ and contributing an energy about 40 kcal towards the molecular stabilization of 1-(Benzenesulfonyl)-2-Methyl-1*H*-Indole-3-Carbaldehyde.

Table 5. Energies associated with delocalization of electron density using the second order Perturbation theory

S.No	Donor NBO (i)	Acceptor NBO (j)	E(2) kcal/mol	E(j)-E(i) a.u	F(i,j) a.u
1	LP(1)N7	BD*(2)C8-C9	44.49	0.42	0.122
2	LP(1)N7	BD*(2)C10-C15	29.67	0.41	0.102
3	LP(3)O20	BD*(1)N7-S19	36.98	0.42	0.115
4	LP(3)O21	BD*(1)N7-S19	40.68	0.42	0.121
5	BD*(2)C10-C15	BD*(2)C13-C14	222.76	0.02	0.095
6	BD*(2)C17-C18	BD*(2)C8-C9	127.56	0.01	0.084

4.4. FT-IR spectral analysis

The representative FT-IR spectrum of 1-(Benzenesulfonyl)-2-Methyl-1*H*-Indole-3-Carbaldehyde is shown in the **Figure 8a**. Similarly, the simulated vibrational spectrum of the same by using the DFT model CAM-B3LYP/6-311++G (d p) in aqueous phase is shown in **Figure 8b**. Another DFT model B3LYP/6-311++G (d p) also been utilized for the frequency calculations. The former model produces a result almost similar to that of experimental observations [31-32]. The calculated harmonic vibrational frequencies are scaled down by a factor of 0.9613 in order to attain a reasonable agreement between those observed and theoretically estimated vibrational frequencies [33]. Most prominent vibrational frequencies and their assignments are presented in the **Table 6a**. Similarly, the complete vibrational frequency assignments are presented in the **Table 6b**.

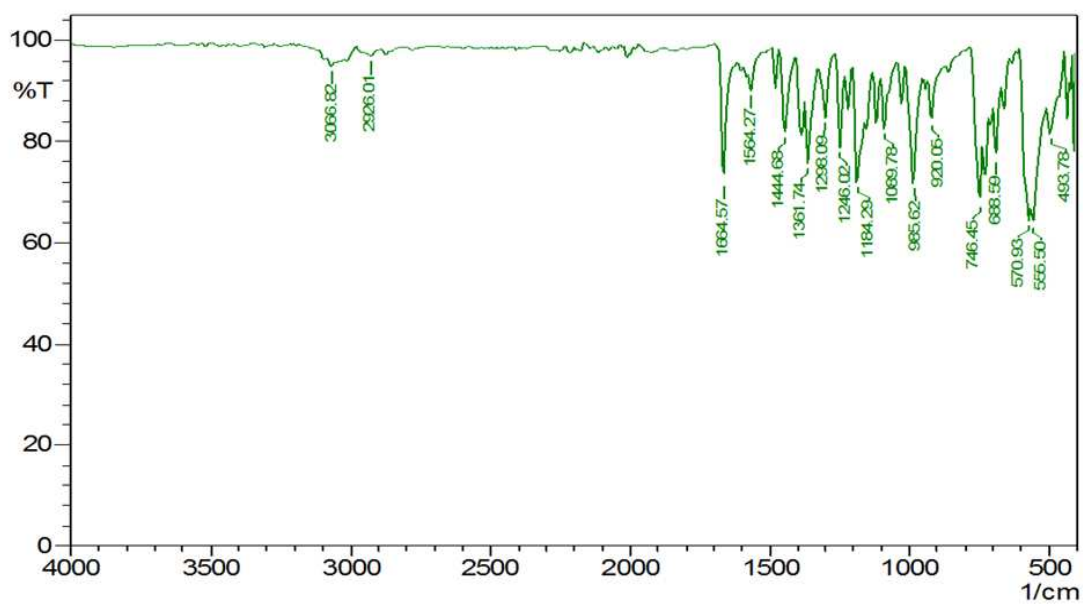


Figure 8a. Experimental FT-IR Spectrum of 1-(Benzenesulfonyl)-2-Methyl-1H-Indole-3-Carbaldehyde

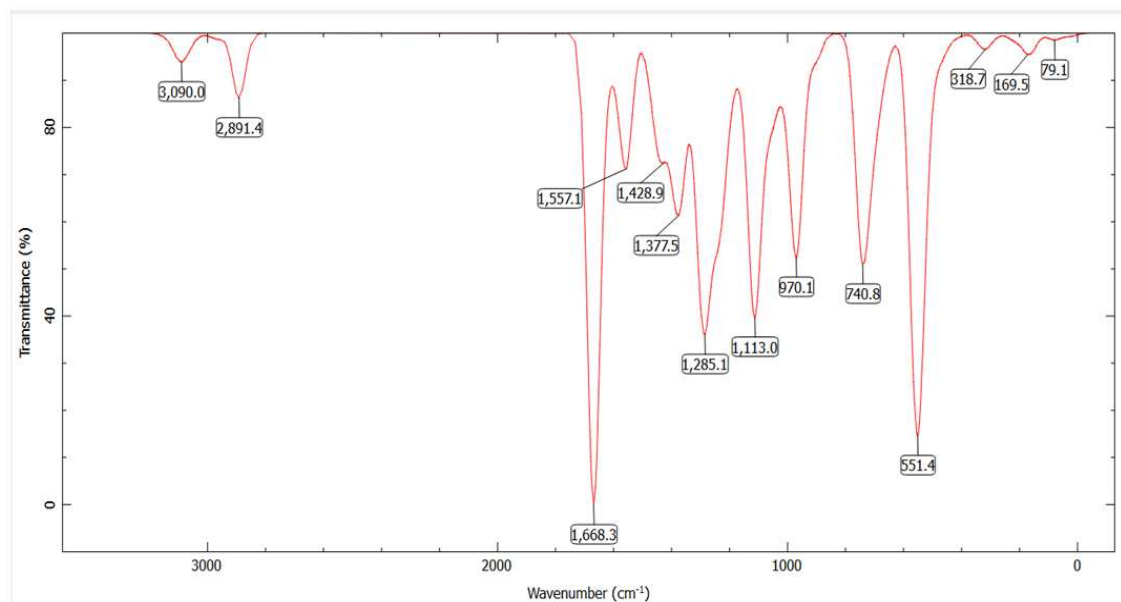


Figure 8b. Simulated vibrational spectrum of 1-(Benzenesulfonyl)-2-Methyl-1H-Indole-3-Carbaldehyde using CAM-B3LYP/6-311++G(d,p) model

Table 6a. Most prominent vibrational frequencies and their assignments by comparing both experimental and theoretical methods

S.No	FT-IR (cm ⁻¹)	CAM-B3LYP/6-311++G (d p) in H ₂ O	B3LYP/6-311++G (d p) in H ₂ O	Assignment
1	3066	3090	3073	Aliphatic CH stretching
2	2926	2891	2864	Formyl CH stretching
3	1664	1668	1656	C=O stretching
4	1246	1280	1294	C-N stretching
5	920	969	961	Indole breathing mode
6	555	554	540	Sulfonyl scissoring

4.4.1 C=O stretching

The FT-IR spectrum of the title compound clearly shows an intense IR absorption peak at 1664 cm⁻¹ corresponds to the stretching vibrational mode of the aldehydic carbonyl group and the CAM-B3LYP model also produces the similar vibrational frequency at 1668 cm⁻¹. The observed carbonyl frequency is somewhat lower than a typical aldehydic stretching frequency and this can be explained on the basis of bond resonance which can be possible only when the formyl group is coplanar with the indole ring. The DFT model also predicted the same and it is shown evident from the optimized molecular geometry of the title compound.

4.4.2 Formyl C-H and Aliphatic C-H stretching

Similarly, the two distinct vibrational peaks at 3066 and 2926 cm⁻¹ must be the vibrational stretching modes of -CH₃ and -CHO protons, respectively. As expected, the vibrational frequency of aldehydic proton observed in a lower frequency range than the methyl protons. The similar observations are also presented by the chosen DFT models. The CAM-B3LYP model predicts a value of 3090 and 2891 cm⁻¹ for the vibrational stretching modes of -CH₃ and -CHO protons respectively.

Table 6b. Complete vibrational frequency assignments of 1-(Benzenesulfonyl)-2-Methyl-1*H*-Indole-3-Carbaldehyde by comparing both experimental and theoretical methods

S. No.	Calculated vibrational frequencies (cm ⁻¹)		Experimental IR (cm ⁻¹)	ASSIGNMENTS
	CAM-B3LYP/6-311++G (d,p)	B3LYP/6-311++G (d,p)		
1.	11.03274397	-52.3110621		μ-phenyl ring
2.	24.93766008	-38.17476108		π-C ₆ -S-N
3.	44.06128163	-4.21991474		μ-phenyl ring
4.	79.14267544	49.95674227		ω-methyl oop
5.	105.8844072	78.89725555		μ-indole ring
6.	134.428192	113.4454163		ω-methyl oop
7.	161.7287275	140.4963983		μ-methyl
8.	165.9705599	151.9797997		ω-formyl C-H oop
9.	174.7746259	158.4550203		ω-formyl C-H oop
10.	184.4400168	173.9256058		ω-indole ring in-plane
11.	203.9255678	188.7813437		μ-methyl
12.	218.0555242	206.2651797		μ-phenyl ring
13.	269.4972827	259.8598657		ω-SO ₂
14.	283.5643701	276.7853787		ω-methyl in-plane
15.	304.3307573	300.2140861		C-S deformation
16.	318.6928676	303.8901935		ω-S-N
17.	322.6945673	319.2568624		ω-methyl
18.	337.3935172	325.3827466		ω-indole ring oop
19.	400.3010853	386.4058783		ω-C-S
20.	401.5741349	392.010738		μ-phenyl ring
21.	416.3318203	410.109037		μ-indole ring in-plane
22.	430.4185182	415.260163		ω-phenyl C-H oop
23.	460.8419329	448.0378014		ω-phenyl C-H oop
24.	481.6363899	478.7144225		Indole ring deformation
25.	530.2038614	515.8607848		π-SO ₂
26.	554.7103785	540.2315663	555	ω-S-O
27.	562.9930354	554.8898532		ω-formyl C-H
28.	573.5747374	556.8651324		μ-indole ring
29.	607.8733446	603.1480745		μ-indole ring
30.	634.0489669	614.85046		μ-C ₈ -C ₉
31.	650.3535762	644.5435751		ω-indole C-C in-plane
32.	682.9870195	668.946464		ω-phenyl C-C oop
33.	690.7117379	684.0230125		All ring deformation
34.	711.9420484	703.3519678		π-phenyl C-C-C
35.	740.8023893	728.6314661		π-indole C-C-C
36.	745.3771199	731.7488659		ω-indole C-H oop
37.	748.3870463	735.1811875		ω-phenyl C-H oop
38.	763.3419904	744.2601854		ω-indole C-C oop
39.	839.4459965	823.7796904		ω-phenyl C-H oop
40.	869.2531218	850.7147396		ω-indole C-H oop
41.	904.5149516	897.3313489		Indole breathing mode
42.	935.47208	917.2619818		ω-phenyl C-H oop
43.	957.9255486	936.2900502		ω-indole C-H oop
44.	969.0013588	961.3523909	920	Indole breathing mode
45.	985.390178	964.50036		Phenyl C-H deformation
46.	986.5222049	965.273149		Phenyl breathing
47.	988.0905658	967.9733446		ω-formyl C-H
48.	988.8960391	979.8630875		ω-indole C-H oop
49.	1006.444763	984.5258732		ω-phenyl C-H oop
50.	1012.519218	1005.170367		All ring breathing
51.	1016.115056	1010.742255		Phenyl breathing
52.	1019.487201	1012.852308		Indole ring deformation
53.	1025.416499	1014.246001		ω-methyl
54.	1057.508827	1050.852689		C-S deformation

ρ – rocking; ω – wagging; π – scissoring; μ – twisting; oop – out-of-plane.

S. No.	Calculated vibrational frequencies (cm ⁻¹)		Experimental IR (cm ⁻¹)	ASSIGNMENTS
	CAM-B3LYP/6-311++G (d,p)	B3LYP/6-311+G (d,p)		
55.	1075.51609	1071.702037		ω-phenyl in-plane
56.	1102.91737	1096.908572		ω-indole in-plane
57.	1113.585397	1109.085071		C-S vibration
58.	1133.450277	1131.592084		ω-phenyl C-H in-plane
59.	1144.229142	1145.849509		ω-indole C-H in-plane
60.	1155.351286	1149.557243		π-N-C ₈ -C ₉
61.	1162.740319	1160.018206		ω-phenyl C-H
62.	1199.584352	1188.807122		C-N deformation
63.	1235.192058	1226.420195		C ₈ -N-C ₁₅ stretching
64.	1277.59577	1274.627564		SO ₂ asymmetric stretch
65.	1280.738356	1294.307778	1246	C ₁₅ -N stretching
66.	1299.563301	1294.488406		ω-C-H all in-plane
67.	1306.261063	1318.899082		ω-phenyl C-H in-plane
68.	1309.76827	1336.391666		Indole deformation
69.	1360.959898	1351.82476		Methyl deformation
70.	1381.63054	1368.864572		ω-methyl
71.	1395.420581	1385.932165		Formyl C-H vibration
72.	1415.749961	1407.707052		Methyl deformation
73.	1428.034125	1419.886146		μ-methyl
74.	1439.416013	1430.209835		μ-phenyl in-plane
75.	1441.054934	1430.909566		Indole ring vibration
76.	1468.394594	1458.240478		Phenyl deformation
77.	1471.273111	1459.535253		All ring deformation
78.	1557.083747	1547.497375		C ₈ -C ₉ stretching
79.	1590.976878	1575.514368		ω-C-H all in-plane
80.	1593.841745	1576.164687		Phenyl C-C stretching
81.	1598.198933	1581.897111		Phenyl C-C stretching
82.	1614.62332	1594.754114		Indole C-C stretching
83.	1668.321538	1656.856402	1664	Carbonyl stretching
84.	2891.436207	2864.492699	2926	Formyl C-H stretching
85.	2964.981329	2948.568477		Aliphatic C-H stretching
86.	3024.803797	3004.286675		Aliphatic C-H asymmetric
87.	3063.426236	3044.626861		Aliphatic C-H asymmetric
88.	3076.223061	3059.100866		Aromatic C-H stretching
89.	3079.144067	3061.931318		Aromatic C-H stretching
90.	3086.598949	3069.399177		Aromatic C-H asymmetric
91.	3090.038000	3073.129309	3066	Aromatic C-H asymmetric
92.	3094.278198	3077.357876		Phenyl C-H vibration
93.	3100.800715	3084.029106		Indole C-H vibration
94.	3104.907292	3088.025518		Phenyl C-H asymmetric
95.	3111.743289	3095.076269		Phenyl C-H asymmetric
96.	3140.177004	3123.210636		Indole C ₁₄ -H stretching

ρ – rocking; ω – wagging; π – scissoring; μ – twisting; oop – out-of-plane.

4.4.2 Formyl C-H and Aliphatic C-H stretching

Similarly, the two distinct vibrational peaks at 3066 and 2926 cm⁻¹ must be the vibrational stretching modes of -CH₃ and -CHO protons, respectively. As expected, the vibrational frequency of aldehydic proton observed in a lower frequency range than the methyl protons. The similar observations are also presented by the chosen DFT models. The CAM-B3LYP model predicts a value of 3090 and 2891 cm⁻¹ for the vibrational stretching modes of -CH₃ and -CHO protons respectively.

4.4.3 S=O stretching

The vibrational frequency observed at 555 cm^{-1} could be the bending mode of sulfonyl S=O bond which is further confirmed from the predicted vibrational frequency.

4.4. UV-Visible spectral analysis

The experimental UV-Visible spectrum of the title compound shows a two distinct absorption maxima at 290 and 227 nm. The former has the least intensity compared to that of the later. The absorption spectrum of 1-(Benzenesulfonyl)-2-Methyl-1*H*-Indole-3-Carbaldehyde shown in **Figure 9a**. Absorbance maxima at 290 nm could more probably be due to the π - π^* transition involving the indole moiety. The characteristics absorption of indole is centered at 270 nm. In this case, λ_{max} shifts towards longer wave-length which could be due to the bathochromic effect of the methyl substituent at position-2 and as well as due to an extension of pi-conjugation over the formyl group at position-3 on the indole ring.

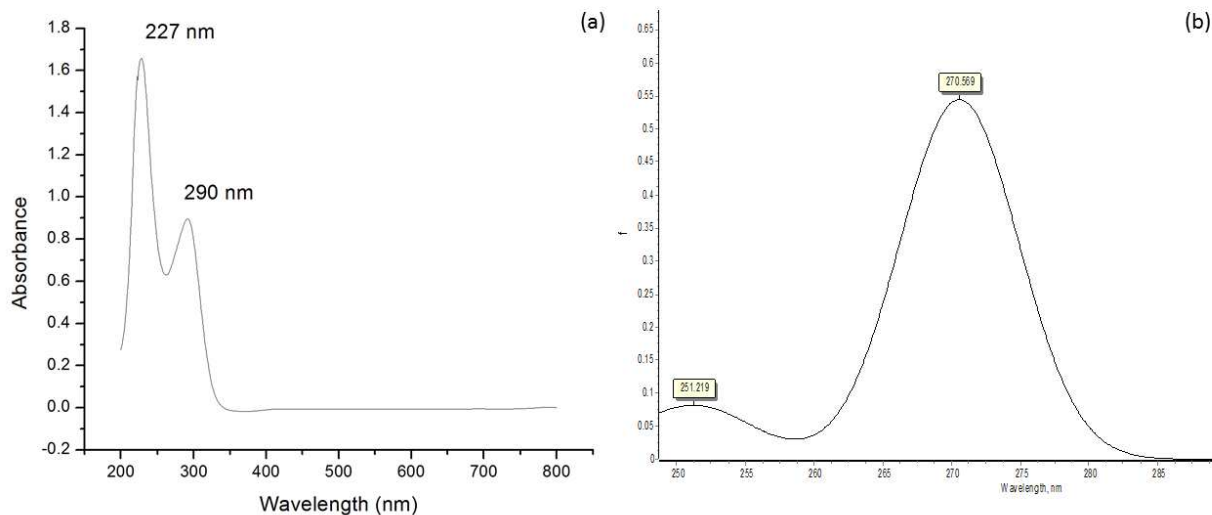


Figure 9a. Observed UV-VISIBLE spectrum and **b.** Calculated absorption spectrum of the title compound

Similarly, the absorbance peak at 227 nm could arise from the π - π^* transition involving the phenyl ring. The high peak intensity suggested that n- π^* transition involving the lone pair of electrons on the Hetero-atoms viz. O and N becomes least favorable. Since, the n- π^* transitions are generally known to be forbidden transitions with very less intensities associated with it.

The theoretical absorbance spectrum of the title compound is derived out of Time-dependent DFT model CAM-B3LYP6-311++G (d p) in aqueous phase. Also, two more DFT models are employed for the same purpose viz. B3LYP6-311++G (2d p) and BVP86/6-311++G (d p) methods. But the later models shows large deviation from the observed experimental results. The CAM-B3LYP model predicts a fairly good absorption maxima for the title compound which has also some deviation from the experimental results. The simulated absorption spectrum, shown in **Figure 9b**, has maximum peak intensities at 271 and 250 nm corresponding to that of experimental absorbance maxima at 290 and 227 nm, respectively. Moreover, the molecular orbitals involving the transition corresponding to λ_{\max} at 271 nm are found to be the HOMO/LUMO and HOMO/SUMO. Similarly, the absorption at 250 nm is found to be more complex to account for and it comprises of several molecular orbitals viz. HOMO, LUMO, SUMO and other higher anti-bonding orbitals having pi-symmetry. Nevertheless, the model produces a good correlation with that of experimental results. The discrepancy between the experimental and theoretical values could be due to the shortsightedness of the chosen DFT model and expected a tolerance limit of 15 nm. The predicted electronic excitation from CAM-B3LYP model can be visualized from the charge densities between ground and excited state. **Figure 10** shows a representation of the difference electron density between the excited and ground state [34].

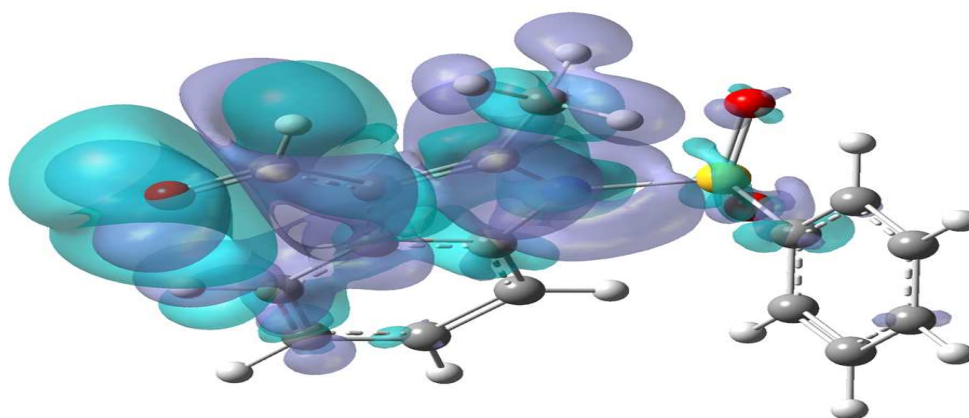


Figure 10. Representation of the difference electron density between the ground and an excited state

It can be easily seen that the electron density moves from the pale green region to the blue region when moving from the ground state to the first excited state. Thus, for most part, the predicted electronic transition can be stated as an excitation of electrons originating mainly from the formyl substituent on the indole ring and also arriving mainly at the same indole ring.

4.5 NMR Spectroscopy

4.5.1 ^1H NMR spectrum

The obtained experimental ^1H NMR spectrum of 1-(Benzenesulfonyl)-2-Methyl-1*H*-Indole-3-Carbaldehyde in CDCl_3 is shown in the **Figure 11a**. Similarly, the NMR shielding tensors of single point geometry of the title compound is calculated by GIAO method employing the same DFT model as mentioned earlier for geometry optimization and also by using another DFT model B3LYP/6-31+G (2d p) in DMSO as solvent. The predicted NMR spectrum of the title compound is shown in **Figure 11b**. For comparison, the CAM-B3LYP shows a very good correlation with the experimental results. Standard reference of TMS shielding tensors computed at B3LYP/6-31+G (2d p) level is utilized in the calculations.

The experimental spectrum of 1-(Benzenesulfonyl)-2-Methyl-1*H*-Indole-3-Carbaldehyde shows a clusters of absorption peaks over the region 7.0 to 8.5 ppm which must arise due to the presence of aromatic protons on the periphery of both the phenyl and indole ring. Similar observations are also predicted by the theoretical methods. Most importantly, the proton resonating at 2.94 ppm with peak area integrated to 3 unit must be the CH₃ protons at position-2 on the indole ring. Also, the CAM-B3LYP model predicted a shielding tensor value of 3.08 ppm for the same. Similarly, the more strongly deshielded proton resonating at 10.30 ppm must be the aldehydic proton of formyl moiety at position-3 on the indole ring. Here also the chosen theoretical model predicted a value of 10.4 ppm for the same proton which is almost equivalent to the experimental result.

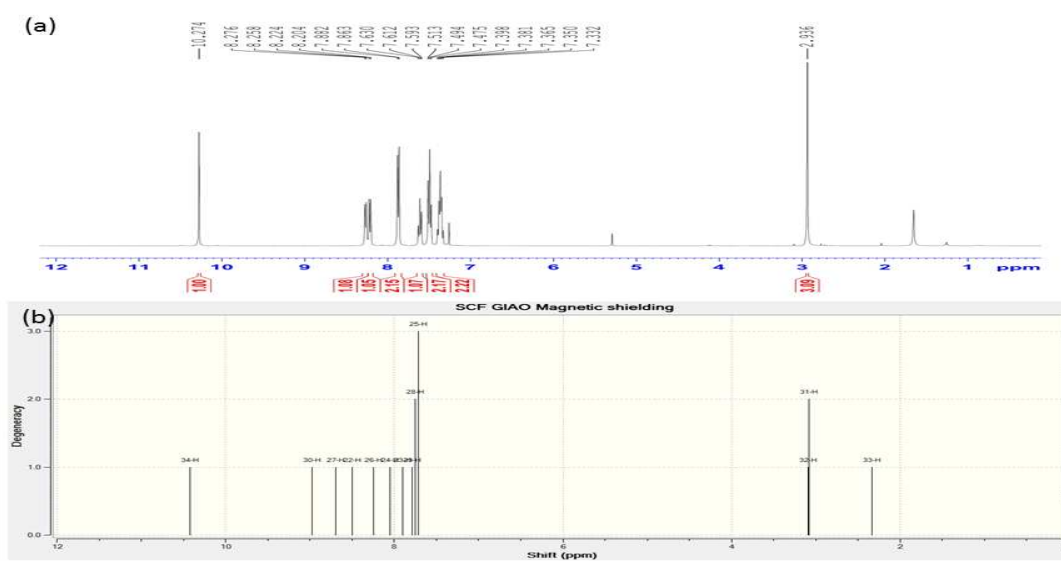


Figure 1 a. Experimental and b. Theoretical ¹H NMR spectrum from GIAO method

From these observations, it is clearly seen that the proposed CAM-B3LYP model for the title compound and its derivatives is an appropriate choice of theoretical method for such NMR predictions. The experimental and theoretical values computed at CAM-B3LYP and B3LYP model for the title compound is presented in the **Table 7**.

Table 7. Experimental and theoretical ^1H NMR chemical shifts (ppm) of 1-(Benzenesulfonyl)-2-Methyl-1*H*-Indole-3-Carbaldehyde

S.No	PROTON	Experimental, CDCl ₃ Chemical shifts (ppm)	CAM-B3LYP/ 6-311++g(d,p)	B3LYP/ 6-311+g(2d,p)
			DMSO	DMSO
1	Methyl	2.93	3.09	3.16
2	Formyl	10.27	10.42	10.57

4.5.2 ^{13}C NMR spectrum

The experimental spectrum of 1-(Benzenesulfonyl)-2-Methyl-1*H*-Indole-3-Carbaldehyde is shown in the **Figure 12**. Similarly, the ^{13}C nuclear magnetic shielding tensors are computed by utilizing a two different DFT models viz. CAM-B3LYP and B3LYP models.

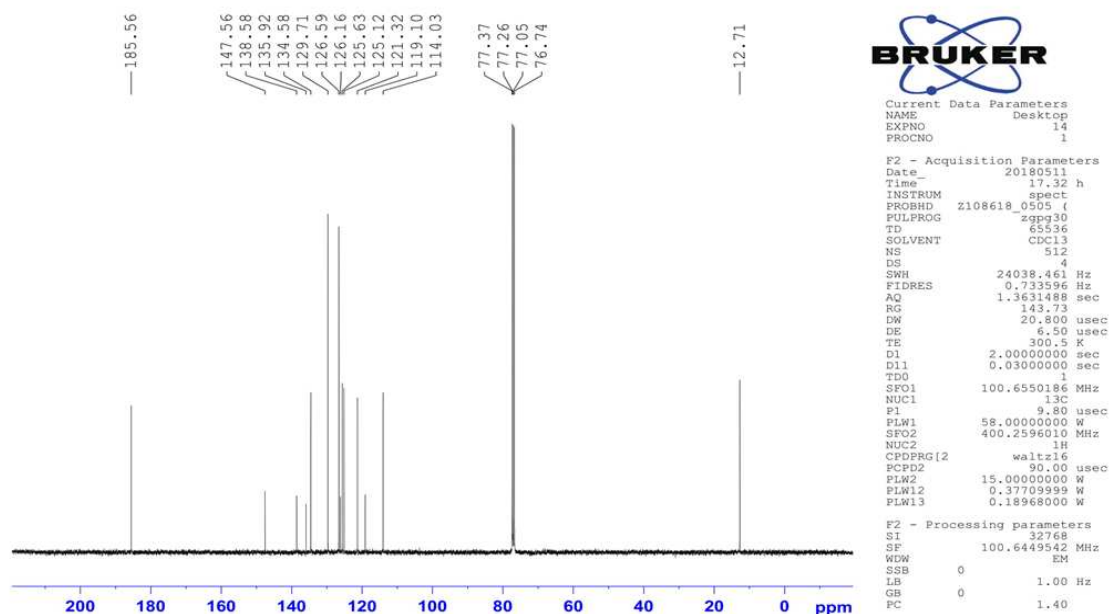


Figure 12. Experimental ^{13}C NMR spectrum of 1-(Benzenesulfonyl)-2-Methyl-1*H*-Indole-3-Carbaldehyde

Like ^1H NMR spectrum of the title compound, the theoretical model B3LYP/6-311+G(2d p) shows a reliable correlation with that of the obtained experimental results. In this

case, the CAM-B3LYP model predicts a value somewhat slightly higher for sp^2 C-atom and slightly a lower value for sp^3 C-atom. The spectrum displays two distinct resonating peaks; one at a far downfield region of about 186 ppm and another one at an up-field region of about 12 ppm. The former is the characteristics radio-frequency absorption peak of sp^2 C-atom of the carbonyl group in aldehydic form. The peak appearing at 12 ppm corresponds to the sp^3 C-atom of the methyl substituent at position-2 on the indole ring. DFT model B3LYP/6-311+G (2d p) predicts almost a similar value for the above mentioned C-atoms i.e. 191 ppm for the carbonyl C-atom and 12 ppm for the methyl substituent. Other sp^2 ring C-atoms are found to be resonating between the regions 110 to 160 ppm. Similar resonating peaks are obtained experimentally for the sp^2 ring C-atoms.

4.6. Docking studies

The main objective of the molecular docking studies using **AUTODOCK 4.2** tools is to evaluate the nature of binding mode, efficiency and types of possible interaction associated with the title compound, if it could become a potent anti-bacterial against Gram positive and Gram negative pathogens. For docking purpose, the first NEAT domain of IsdH protein of Gram positive *Staphylococcus Aureus* and N-terminal domain of Gram negative *Neisseria Meningitidis* PilB has been chosen and their respective PDB ID's are **3S48** and **2FY6**. The tertiary structure of the chosen receptor protein molecules are shown in the **Figure 13a & b**. It is well known that the protein targets viz. 3S48 and 2FY6 are primarily expressed during the human infection. Both can acts as a cellular adhesion to the human ligands [35-40].

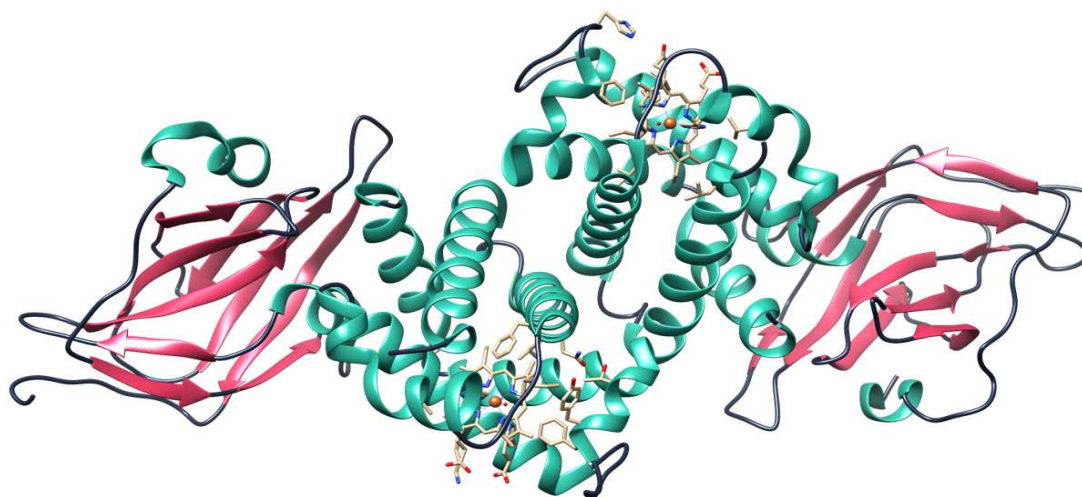


Figure 13a. Quaternary structure of the target protein 3S48 of Gram positive S.Aureus

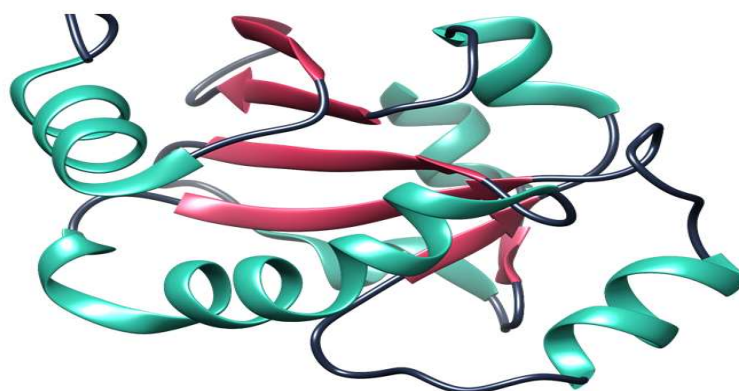


Figure 13b. Tertiary structure of the target protein 2FY6 of Gram negative N.Meningitidis PilB

Before docking, the residual water molecules are eliminated from the target receptors. All the polar H's are added, non-bonded atoms and non-polar H's are allowed to merge. The Kollman charges of 18.3 and 4.0 are added to the receptor protein 3S48 and 2FY6, respectively. Similarly, the ligand molecule is defined and added with Gasteiger partial charges. All possible rotatable bonds are set to be free and Torsional Degrees Of Freedom (TORSDOF) is only 3 for the ligand molecule, 1-(Benzenesulfonyl)-2-Methyl-1*H*-Indole-3-Carbaldehyde. On the other hand, the protein is considered to be a rigid substrate during the docking processes. The individual docking results of the title compound involving the

two separate receptor proteins 3S48 and 2FY6 are given in the **Table 8a & b** respectively. As given in the above table, the Gibb's free energy of binding is found to be a large negative value of about 6.24 kcal for the docking process between the ligand and the receptor 2FY6 which indicate the spontaneity of the process is slightly far better than the one between the same ligand with the protein 3S48. The later has energy value of only about -5.69 kcal. It should be mentioned that the docking conformation of the ligand with the receptor protein 2FY6 has no H-bonding interactions though it has large negative value of binding when compared to that of the binding energy between the same ligand and the NEAT domain of S.Aureus.

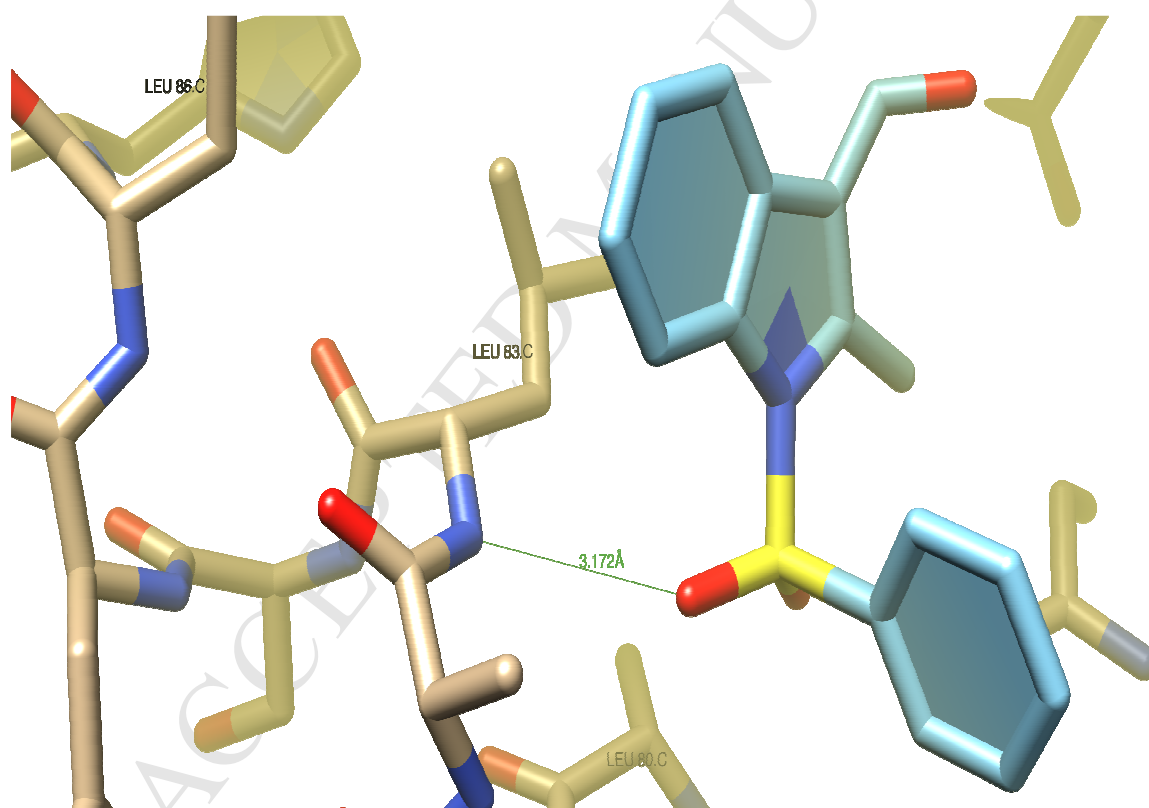


Figure 14. Docking conformation showing the H-bonding interaction between the ligand and the target receptor 3S48

On the other hand, the docking conformation of ligand with the target protein 3S48 shows H-bonding interaction between the acceptor O-atom of the ligand and the donor N-atom

on residue Leucine-83 of the receptor protein, shown in the **Figure 14**. Bond length between the donor and an acceptor atom is found to be 3.172 Å. Here, it should be emphasized that an active pharmacological ingredient must exert both kind of binding forces viz. polar and non-polar interactions.

Table 8a. Estimated free energy, inhibition constant, electrostatic energy and total intermolecular energy obtained from ligand-protein interactions between the target receptor 3S48 and 1-(Benzenesulfonyl)-2-Methyl-1*H*-Indole-3-Carbaldehyde.

S.NO	Binding energy (Kcal/Mol)	Ligand efficiency	Inhibition constant K_i (μ M)	Intermolecular energy (Kcal/Mol)	Vdw + H-bonding + desolv. Energy (Kcal/Mol)	Electrostatic energy (Kcal/Mol)	Total internal energy	Torsion. energy (Kcal/Mol)
1	-5.69	-0.27	67.47	-6.59	-6.29	-0.3	-0.81	0.89
2	-5.38	-0.26	113.13	-6.28	-6.17	-0.11	-0.85	0.89
3	-5.29	-0.25	133.54	-6.18	-6.26	0.08	-0.83	0.89
4	-5.22	-0.25	148.55	-6.12	-6.06	-0.05	-0.78	0.89
5	-5.00	-0.24	217.59	-5.89	-5.85	-0.04	-0.96	0.89
6	-4.78	-0.23	315.50	-5.67	-5.58	-0.09	-0.93	0.89
7	-4.54	-0.22	473.26	-5.43	-5.28	-0.16	-0.86	0.89
8	-4.46	-0.21	539.17	-5.35	-5.36	0.00	-0.81	0.89
9	-4.38	-0.21	610.94	-5.28	-5.19	-0.09	-0.95	0.89
10	-4.01	-0.19	1.15 (mM)	-4.91	-4.88	-0.02	-1.00	0.89

On the basis of inter-molecular interactions as mentioned earlier, it has been concluded that the binding efficiency of the ligand on the receptor surface is found to be better in the case of Gram positive bacteria *S.Aureus* than the Gram negative *N.Meningitidis*.

Table 8b. Estimated free energy, inhibition constant, electrostatic energy and total intermolecular energy obtained from ligand-protein interactions between the target receptor 2FY6 and 1-(Benzenesulfonyl)-2-Methyl-1*H*-Indole-3-Carbaldehyde.

S.NO	Binding energy (Kcal/Mol)	Ligand efficiency	Inhibition constant K_i (μ M)	Intermolecular energy (Kcal/Mol)	Vdw + H-bonding + desolv. Energy (Kcal/Mol)	Electrostatic energy (Kcal/Mol)	Total internal energy	Torsion. energy (Kcal/Mol)
1	-6.24	-0.30	26.68	-7.13	-7.08	-0.06	-0.84	0.89
2	-6.17	-0.29	30.22	-7.06	-6.97	-0.09	-0.94	0.89
3	-5.92	-0.28	45.60	-6.82	-6.75	-0.07	-0.94	0.89
4	-5.82	-0.28	54.11	-6.72	-6.76	0.05	-0.97	0.89
5	-5.67	-0.27	70.40	-6.56	-6.44	-0.12	-0.95	0.89
6	-5.49	-0.26	93.80	-6.39	-6.36	-0.03	-0.85	0.89
7	-5.47	-0.26	97.36	-6.37	-6.34	-0.03	-0.92	0.89
8	-5.36	-0.26	116.83	-6.26	-6.10	-0.16	-0.82	0.89
9	-4.39	-0.21	601.90	-5.29	-5.19	-0.1	-0.89	0.89
10	-3.74	-0.18	1.81 _(mM)	-4.64	-4.62	-0.02	-0.86	0.89

5. Conclusion

An N-Substituted 1*H*-indole derivative was synthesized, in presence of a phase transfer catalyst of type quaternary ammonium salt in basic conditions. Then the compound was characterized by using FT-IR, UV-Visible and NMR spectroscopic methods and effectively compared with DFT studies in arriving at the structural characteristics of 1-(Benzenesulfonyl)-2-Methyl-1*H*-Indole-3-Carbaldehyde. The CAM-B3LYP model predicted a ground state energy of about -1295.90 Hartrees in aqueous phase and found to be more stabler than the title compound in gas phase by means of solvation energy of about 100.4 kcal. The optimized structure shows a co-planar

formyl group with an indole ring which could result in an extensive conjugation and it is confirmed from the bond length of 1.45 Å between C₇-C₁₉ atoms. Moreover, the sulfonyl S-atom has nuclear charge of about 2.265 far greater than that of the nucleophilic carbonyl C-atom having the value of only 0.36. The energy gap was calculated and found to be 7.13 e V. NBO analysis revealed that the valence Lewis-type NBO's contribute only 97% of its total electron densities to the natural Lewis structure which was slightly lesser than expected. Also, the delocalization of anti-bonding electron pair from C₁₀-C₁₅ to an anti-bonding orbital of C₁₃-C₁₄ provides a higher stabilization energy of about 222.8 kcal/mol among other perturbations within the title compound. Vibrational analysis showed that the observed carbonyl frequency is somewhat lower than a typical aldehydic stretching frequency and it could be possible only when the formyl group is coplanar with the ring. Similarly, the absorbance maxima at 290 nm could more probably be due to the π - π^* transition involving the indole moiety and the bathochromic effect can be explained by the methyl substituent at position-2 and an extension of pi-conjugation over the formyl group at position-3 on the indole ring. From the NMR spectra, it was evident that the strongly deshielded proton resonating at 10.30 ppm must correspond to the aldehydic proton at position-3 on the indole ring. The chosen theoretical model also predicted a value of 10.4 ppm for the same proton which is almost equivalent to the experimental result. From the molecular drug docking studies of the title compound, the docking conformation of ligand with the target protein 3S48 shows H-bonding interaction between the acceptor O-atom of the ligand and the donor N-atom on residue Leucine-83 of the receptor protein whereas the molecular interaction between the ligand and receptor protein of N.Meningitidis has no such H-bond's. Hence, it has been predicted theoretically that the binding efficiency of the ligand on the target receptor surface was found to be better in the case of Gram positive bacteria S.Aureus than the Gram negative N.Meningitidis.

6. References

- [1] H. Kusama, M. Kurashige, H. Arakawa, *Journal of Photochemistry and Photobiology A: Chemistry*, 169 (2005) 169–176.
- [2] A. H. Mandour, E. R. El-sawy, K. H. Shaker, M. A. Mustafa, *Acta Pharm.* 60 (2010) 73–88.
- [3] A. Andreani, S. Burnelli, M. Granaiola, A. Leoni, A. Locatelli, R. Morigi, M. Rambaldi, L. Varoli, L. Landi, C. Prata, M. V. Berridge, C. Grasso, H. H. Fiebig, G. Kelter, A. M. Burger, M. W. Kunkel, *J. Med. Chem.* 51 (2008) 4563–4570.
- [4] M. Giampieri, A. Balbi, M. Mazzeia, P. L. Colla, C. Ibba, R. Loddo, *Antiviral Research* 83 (2009) 179–185.
- [5] S. Lee, K. Y. Yi, S. K. Kim, J. Suh, N. J. Kim, S. E. Yoo, B. H. Lee, H. W. Sao, S. O. Kim, H. Lim, *Eur J Med Chem* 38 (2003) 459.
- [6] R. Ragno, A. Coluccia, G. La Regina, G. De Martino, F. Piscitelli, A. Lavecchia, E. Novellino, A. Bergamini, C. Ciaprini, A. Sinistro, G. Maga, E. Crespan, M. Artico, R. Silvestri, *J. Med. Chem.* 49 (2006) 3172–3184.
- [7] N. Simon, J. Young, *Psychiatry Neurosci.* 32 6 (2007) 394–399.
- [8] F. J. Huff, P. G. Antuono, J. E. Delagandara, M. A. McDonald, N. R. Cutler, S. R. Cohen, R. C. Green, F. P. Zemlan, M. L. Crismon, M. Alter, J. E. Shipley, W. E. Reichman, *Alzheimer Disease and Associated Disorders* 10 2 (1996) 93–102.
- [9] R.B. Van Order, H.G. Lindwall "Indole". *Chem. Rev.* 30 (1942) 69–96.
- [10] Brieger, Ludwig "Ueber die flüchtigen Bestandtheile der menschlichen Excremente" ("On the volatile components of human excrement"), *Berichte der deutschen chemischen Gesellschaft*, 10 (1877) 1027–1032.
- [11] H. Wang, T. Ng. *Comparative Biochemistry and Physiology Part C.*, 132 (2002) 261–268.

- [12] U. P. Singh, B. K. Sarma, P. K. Mishra, A. B. Ray. *Folia Microbiol (Praha)* 45(2) (2000) 173-6.
- [13] A. Brayfield, *Martindale: The Complete Drug Reference*, London, UK, Pharmaceutical Press, 2014.
- [14]. H. H. Keasling, R. E. Willette, and J. Szmuszkovicz *J. Med. Chem.*, 7 (1) (1964) 94–96.
- [15] M.J. Frisch, G.W. Trucks, H.B. Schlegel, G.E. Scuseria, M.A. Robb, J.R. Cheeseman, J.A. Montgomery Jr., T. Vreven, K.N. Kudin, J.C. Burant, J.M. Millam, S.S. Iyengar, J. Tomasi, V. Barone, B. Mennucci, M. Cossi, G. Scalmani, N. Rega, G.A. Petersson, H. Nakatsuji, M. Hada, M. Ehara, K. Toyota, R. Fukuda, J. Hasegawa, M. Ishida, T. Nakajima, Y. Honda, O. Kitao, H. Nakai, M. Klene, X. Li, J.E. Knox, H.P. Hratchian, J.B. Cross, C. Adamo, J. Jaramillo, R. Gomperts, R.E. Stratmann, O. Yazyev, A.J. Austin, R. Cammi, C. Pomelli, J.W. Ochterski, P.Y. Ayala, K. Morokuma, G.A. Voth, P. Salvador, J.J. Dannenberg, V.G. Zakrzewski, S. Dapprich, A.D. Daniels, M.C. Strain, O. Farkas, D.K. Malick, A.D. Rabuck, K. Raghavachari, J.B. Foresman, J.V. Ortiz, Q. Cui, A.G. Baboul, S. Clifford, J. Cioslowski, B.B. Stefanov, G. Liu, A. Liashenko, P. Piskorz, I. Komaromi, R.L. Martin, D.J. Fox, T. Keith, M.A. Al-Laham, C.Y. Peng, A. Nanayakkara, M. Challacombe, P.M.W. Gill, B. Johnson, W. Chen, M.W. Wong, C. Gonzalez, J.A. Pople, *Gaussian 03, Revision B.03*, Gaussian, Inc., Pittsburgh PA, 2003.
- [16] A.D. Becke, *J. Chem. Phys.* 98 (1993) 5648–5652.
- [17] C. Lee, W. Yang, R.G. Parr, *Phys. Rev. B* 37 (1988) 785–789.
- [18] Takeshi Yanai, David P. Tew, Nicholas C. Handy. *Chemical Physics Letters*, 393 (2004) 51–57.
- [19] Bryan M. Wong, Timothy H. Hsieh. *J. Chem. Theory Comput.* 2010, 6, 3704–3712

- [20] K. A. Nguyen, P. N. Day, R. Patcher. *Journal of Chemical Physics* 135, 074109 (2011)
- [21] J.P. Doering. *J. Chem. Phys.*, 51 (1969) 2866.
- [22] T.M. Duncan. *Principal Components of Chemical Shift Tensors: A compilation*; 2nd ed.; Farragut Press: Madison, WI, 1997.
- [23] Morris, G. M., Huey, R., Lindstrom, W., Sanner, M. F., Belew, R. K., Goodsell, D. S. and Olson, A. J. (2009) *J. Computational Chemistry*, 16 (1996) 2785-91.
- [24] E.F. Pettersen, T.D. Goddard, C.C. Huang, G.S. Couch, D.M. Greenblatt, E.C. Meng, T.E. Ferrin. *J Comput Chem.* 25(13) (2004)1605-12.
- [25] G.J. Kirkwood. *J. Chem. Phys.*, 2 (1934) 351.
- [26] L. Onsager. *J. Am. Chem. Soc.*, 58 (1936) 1486-93.
- [27] P. Pulay, G. Fogarasi. *J. Chem. Phys.*, 96 (1992) 2856-60.
- [28] F.M. Anne, K.J. Whitesell, *Organische Chemie: Grundlagen, Mechanismen, Bioorganische. Anwendungen*, Springer (1995) ISBN 978-3-86025-249-9.
- [29] P. Politzer, P. Lane, *Struct. Chem.* 1 (1990) 159–164.
- [30] J.P. Foster, F. Weinhold. *J. Am. Chem. Soc.*, 102 (1980) 7211-18.
- [31] L.J. Bellamy, *The infrared spectra of complex molecules*, Vol. 1, 3rd edn., Halsted Press, John Wiley and Sons, New York, 1975, p. 433.
- [32] N.B. Colthup, L.H. Daly, S.E. Kimberley, *Introduction to infrared and Raman spectroscopy*, 2nd edn., Academic Press, New York, 1975.
- [33] W.M. Wong. *Chem. Phys. Lett.*, 256 (1996) 391-99.
- [34] G. Scalmani, M.J. Frisch, B. Mennucci, J. Tomasi, R. Cammi, V. Barone. *J. Chem. Phys.*, 124 (2006) 094107: 1-15.

- [35] H. Deokar, J. Chaskar, A. Chaskar, *J. Heterocyclic Chem.*, 51 (2014) 719.
- [36] J.T. Foster, Surface protein adhesins of staphylococci, p. 3-26. *In* M. Wilson (ed.), *Bacterial adhesion to host tissues: mechanisms and consequences*. Cambridge University Press, Cambridge, United Kingdom, 2002.
- [37] S.R. Clarke and S. J. Foster. Surface adhesins of *Staphylococcus aureus*. *Adv. Microb. Physiol.* 51 (2006) 187-224.
- [38] D.S. Stephens, B. Greenwood, P. Brandtzaeg. Epidemic meningitis, meningococcaemia, and *Neisseria meningitidis*. *Lancet* 369 (2007) 2196–2210.
- [39] R.C. Read, A. Fox, K. Miller, T. Gray, N. Jones, R. Borrows, D.M. Jones, R.G. Finch. Experimental infection of human nasal mucosal explants with *Neisseria meningitidis*. *J. Med. Microbiol.* 42 (1995) 353–361.
- [40] C.F. Rayner, A. Dewar, E.R. Moxon, M. Virji, R. Wilson. The effect of variations in the expression of pili on the interaction of *Neisseria meningitidis* with human nasopharyngeal epithelium. *J. Infect. Dis.* 171 (1995) 113–121.

Research Highlights

- N-Substituted 1H-indole derivative was synthesized.
- FT-IR, UV-Visible and NMR spectral analysis were carried out by joint experimental and theoretical studies.
- NBO and Molecular docking studies of the title compound were reported for the first time.
- Optical absorption properties were elaborately discussed and justified.